Pergamon

0967-0637(95)00037-2

Deep-Sea Research I, Vol. 42, No. 8, pp. 1423–1451, 1995

0967-0637/95 $9.50 + 0.00

A new depth–time equation for Sippican or TSK *T*-7, *T*-6 and *T*-4 expendable bathythermographs (XBT)

K. HANAWA,* P. RUAL,† R. BAILEY,‡ A. SY§ and M. SZABADOS‖

(*Received* 14 *February* 1994; *in revised form* 24 *September* 1994; *accepted* 25 *November* 1994)

Abstract—A new depth–time equation for Sippican and Tsurumi-Seiki (TSK) *T*-7, *T*-6 and *T*-4 type expendable bathythermographs (XBTs) is presented based on the results of an internationally co-ordinated set of controlled XBT and conductivity–temperature–depth (CTD) comparison experiments. The experiments were geographically distributed over as many different oceanic water masses as possible to assess the possible influence that variations in the density and viscosity of the water column may have on the XBT fall rate. A newly developed temperature-error-free method is applied to the data set to obtain the depth-difference information between the CTD and the uncorrected XBT data. The accuracies in depth were found in general to be outside of the manufacturers' specified accuracies. The mean depth error for the *T*-7 type of probe was found to be about +25 m at 750 m, whereas the manufacturers' depth-accuracy specification at 750 m is only ±15 m. Since the *T*-4/*T*-6 and the *T*-7 data sets were found not to be statistically different at the 95% confidence level, a unique new Sippican–TSK *T*-4/*T*-6/*T*-7 depth–time equation is determined: $Z_{467} = 6.691\,t - 0.00225\,t^2$. Yet, even with a mean depth perfectly corrected, the individual scatter of the probes is shown to be largely outside the manufacturers' specifications. No discernible effect of the water mass characteristics of the onboard equipment or of the type of manufacturer, was generally found on the fall rate of the probes. Finally an approximate linear correction formula is given for correcting depths recorded using the manufacturers' original depth–time equation: $Z_1 = 1.0336\,z$. But, until an international mechanism is established to implement the general use of the new equation, it is of the utmost importance not to use the new reference equation when archiving or exchanging XBT data. The mixing of data in the data archives must be absolutely avoided.

INTRODUCTION

In recent times expendable oceanographic probes, in particular expendable bathythermographs (XBTs) launched from ships-of-opportunity, have been a significant component of many large-scale oceanographic research programmes, such as the Tropical Ocean Global Atmosphere (TOGA) Programme and the World Ocean Circulation Experiment (WOCE). These probes will no doubt also be heavily relied upon in future operational oceanographic programmes such as the proposed Global Ocean Observing System

*Tohoku University, Department of Geophysics, Sendai 980, Japan.

†ORSTOM, Surtropac Group, BPA5 Noumea, New Caledonia.

‡Author for correspondence: CSIRO Division of Oceanography, Castray Esplanade, Hobart, Tasmania 7001, Australia.

§Budesamt fuer Seeschiffahrt und Hydrographie, Hamburg 36, Germany.

‖NOAA/NOS-OOES, Silver Spring, MD 20910-3233, U.S.A.

(GOOS), and there will be a growing need to utilize these instruments to the limits of their accuracies.

The depth of the XBT at any particular instant is not directly measured, but is inferred from an assumed fall rate of the probe. When conductivity–temperature–depth (CTD) and XBT measurements are conducted along an observational transect, a pseudo-undulation of the isotherms appears in the vertical temperature cross-section. This is due to the depth error in the XBT data, and its existence has already been pointed out by several authors (e.g. Flierl and Robinson, 1977; Seaver and Kuleshov, 1982; Heinmiller *et al.*, 1983). Several investigators have since estimated revised depth–time (fall rate) equations for the XBT using a number of different techniques (McDowell, 1977; Heinmiller *et al.*, 1983; Green, 1984; Hanawa and Yoritaka, 1987; Henin, 1989; Gould, 1990; Singer, 1990; Sy and Ulrich, 1990; Hanawa and Yoshikawa, 1991; Hallock and Teague, 1992; Hanawa and Yasuda, 1992). In addition, Green (1984) provides a detailed description of the hydrodynamics of XBTs.

The Integrated Global Ocean Service System (IGOSS) Task Team on Quality Control for Automated Systems (TT/QCAS) initiated an international effort to conduct further XBT/CTD comparison tests under controlled experimental conditions, in order to develop accurate new equations for universal use. The probes evaluated were the commonly used Sippican and Tsurumi-Seiki (TSK) *T*-7 (760 m), *T*-6 (460 m) and *T*-4 (460 m) types of XBT, all of which use the same manufacturers' depth–time equation. The co-investigators' initial individual results can be found in a report of the Intergovernmental Oceanographic Commission (1992). The individual new depth–time equations were generally very similar. It was therefore decided to combine all data sets collected by the co-investigators, and to apply the best available depth-error estimation technique (a modification of the independently developed temperature-error-free method of Hanawa and Yasuda, 1992, and Rual, 1991). Full results of this study can be found in UNESCO (1994).

The present paper focuses on the determination of a new unique reference depth–time equation for the Sippican and TSK *T*-4, *T*-6, *T*-7 XBT probes. The possible influences on the fall rate by different water masses, onboard recording equipment, and probe manufacturers are examined. The scatter of the fall rates is compared to the manufacturers' specifications. A depth correction formula is derived for correcting archived data. Finally a review is made of the results obtained by previous investigators, and their results are compared to the new depth–time equation.

XBT/CTD COMPARISON EXPERIMENT

Probe types and manufacturers

The results presented in this paper apply to Sippican or TSK *T*-7 (760 m), *T*-6 and *T*-4 (460 m) models of XBT probes, all of which use the same manufacturers' depth–time equation. The nose cones of the *T*-4 and *T*-6 XBTs are manufactured heavier than those of the *T*-7 to match the *T*-7 in overall weight (more wire on the probe spool), in fall rate characteristics and hence in the depth–time equation. Since the only difference between the *T*-6 and *T*-4 types of XBT is the amount of wire on the ship spool so as to allow the *T*-4 probe to be dropped from faster vessels, these two types of probes are not distinguished between for this study. XBTs made by TSK, manufactured under a Sippican licence, should be identical to the original Sippican probes. Some Sippican Deep Blues (760 m)

were also tested, but as their probes are identical to the probes of the *T*-7, they are not distinguished between for this study and hereafter will be considered as *T*-7.

Locations and descriptions of the data sets

Between 1985 and 1992, XBT/CTD comparison experiments were independently carried out by five institutions and by one manufacturer (see Table 1). For the present analysis, 161 *T*-7 XBT and 211 *T*-4/*T*-6 profiles, for a total of 372 profiles, were collected. In Fig. 1 are shown the locations where the XBT/CTD comparison experiments were conducted. Temperature–salinity (*T*–*S*) relationships, extracted from climatological data (Levitus, 1982), are displayed in Fig. 2 for each region. A 100-m mark has been added to each curve to show the extent of the surface waters. The non-shaded *T*–*S* field represents the open-waters of the World Ocean at depths between 50 and 800 m and salinities between 30 and 39 psu. It shows that the comparison data used in the present study, distributed over various oceans and regions, cover various water masses (S = 34–37 psu, T = 5–30°C) so as to specifically assess the possible influence of the density and viscosity structures on the XBT fall rate (Seaver and Kuleshov, 1982).

Experimental procedures

All XBT data are evaluated relative to a field standard, the CTD profiler (Table 1). Generally, the CTD profilers were calibrated before and after each voyage of the research vessels involved, and the calibration results were applied to the CTD data before analysis. Therefore CTD data errors are at least an order of magnitude smaller than XBT data errors and, for this study, will be considered as negligible. A number of different digital XBT recorders were used to collect the XBT data (Table 1). Each XBT recorder underwent a calibration check before and after each voyage. No strip chart recorders were used for this experiment as this type of recorder is no longer very much in use and may include additional depth errors due to possible variations in the speed of the roller-chart mechanisms. A "side by side, XBT/CTD comparison" was the main improvement in the field procedures used in this study compared to most of the previous investigators' studies. As far as possible, XBTs were dropped during the descent of the CTD so that, at least at some depth, the instruments were coincident in depth. This was in attempt to eliminate as much as possible depth differences due to temperature–field variations in time or space (e.g. internal waves). Generally, XBTs were dropped within 10–15 min of the start of descent of the CTD, so as to coincide with the CTD within the thermocline. Previous investigators had not necessarily compared XBTs that were as close in time as possible (or indeed at precisely the same location) to the CTD.

TEMPERATURE-ERROR-FREE METHOD TO CALCULATE AN XBT DEPTH–TIME EQUATION

Provided that the onboard XBT equipment is working correctly, it is considered that there are two main error-sources in XBT data: (i) depth errors due to an inaccurate depth–time equation for the fall rate of the probes; (ii) temperature errors due to the scatter of thermistor responses and inaccuracies in the conversion of thermistor resistance

Table 1. *Summary of XBT/CTD comparison experiments for T-4, T-6, T-7 XBTs (372 probes)*

Regional and manufacturer's data sets	Number of profiles	'Good' profiles $2/3n_M$	Probe types and manuf.	Field experiments: Date	Field experiments: Institution	XBT recorder	CTD profiler	A	B 10^{-5}	Maximum depth error: metre	Maximum depth error: %	Correl. coef. (AB)	σ_A 10^{-3}	σ_B 10^{-5}	σ_a 10^{-3}	σ_b 10^{-5}
					Manufacturers' equation (6):			6.472	216	−25.9	−3.24					
NW Pac. (*nwp*, 1)	54	50	*T*-6/*T*-7 TSK	1985–87–89 1991–92	TOHOKU	ORI Z–60–II	NB IIIb	6.669	223	−2.4	−0.30	0.87	22	22	154	154
NW Trop. Pac (*nwtp*, 2)	9	9	*T*-7 TSK	1987	TOHOKU	ORI	NB IIIb	6.652	201	−1.6	−0.30	0.78	20	27	61	81
W Equat. Pac. (*wep*, 4)	101	70	*T*-4/*T*-7 Sippican	1989–91–92	ORSTOM	Argos	SBE–9	6.662	201	−0.9	−0.22	0.89	26	46	221	388
SW Trop. Pac. (*swtp*, 5)	76	57	*T*-4/*T*-6/*T*-7 Sippican	1989–91–92	ORSTOM	Argos	SBE–9	6.694	249	−3.4	−0.42	0.84	23	37	170	280
Tasman Sea (6)	12	6	*T*-7 Sippican	1989	CSIRO	Mk–9	NB	6.747	200	10.9	1.36	0.84	69	38	169	93
SE Indian (*sei*, 3)	21	13	*T*-7 Sippican	1987	CSIRO	Mk–9 SA–810	NB	6.666	224	−3.0	−0.37	0.94	29	19	105	68
Bahamas (7)	21	15	*T*-4 Sippican	1992	NOAA/NOS	Mk–9	NBIII	6.514	061	−4.8	−1.35	0.93	32	53	123	205
NW Trop. Atl. (*nwta*, 8)	66	55	*T*-4/*T*-6/*T*-7 Sippican	1988–91	NOAA/NOS	Mk–9	NB III	6.822	293	6.3	1.00	0.73	11	16	85	119
NE Atlant. (*nea*, 9)	12	10	*T*-7 Sippican	1991	SIPPICAN BSH	Argos Mk–12	NB III	6.561	179	−9.1	−1.13	0.92	34	30	108	93
T-7 Sippican	115	83	Sippican	1987–92				6.698	235	−0.7	−0.09	0.82	14	10	131	87
T-4/*T*-6 Sippican	194	143	Sippican	1988–92				6.697	221	0.6	0.13	0.86	18	28	210	340
T-7 TSK	46	42	TSK	1985–91				6.707	242	−0.7	−0.12	0.91	20	15	129	100
T-6 TSK	17	17	TSK	1989–92				6.566	164	−5.7	−1.27	0.97	31	52	129	213
T-4/*T*-6 Global	211	160				New *T*-4/*T*-6 equation (7):		6.683	215	−0.2	−0.06	0.86	16	26	206	329
T-7 Global	161	125				New *T*-7 equation (8):		6.701	238	−0.8	−0.10	0.85	12	8	130	91
T-4/*T*-6/*T*-7	372	285				New *T*-4/*T*-6/*T*-7 Equation (9):		6.691	225	—	—	0.83	10	15	177	254

BSH: Bundesamt fur Seeschiffahrt und Hydrographie (Germany)
CSIRO: Commonwealth Scientific and Industrial Research Organisation, (Australia)
NOAA/NOS: National Oceanic and Atmospheric Administration (U.S.A.)
ORSTOM: Institut Français de Recherche Scientifique pour le Développement en Coopération (France)
TOHOKU: Tohoku University (Japan)
Mk–9: Sippican Mark 9
Mk–12: Sippican Mark 12
SA–810: Bathy-Systems model SA–810
Argos: CLS-Argos/Protecno XBT-ST model 1 and 2
ORI: Ocean Research Institute, Tokyo University
Z–60–II: Murayama Denki
TSK: Tsurumi-Seiki
NB: Neil Brown
NB III: Neil Brown model 3
NB IIIb: Neil Brown model 3b
SBE–9: SeaBird model 9

The field areas are those of Fig. 1. The last 9 columns are, respectively: (i) the mean A and B coefficients of the data set equation, (ii) the maximum absolute depth error between that equation and the new reference equation (7), down to 800 m for *T*-7 probes (or to 450 m for *T*-4/*T*-6 probes), expressed in metres or in percent of its depth, (iii) the correlation coefficient between A and B, (iv) the standard deviation of the mean A, B and individual a, b coefficients.

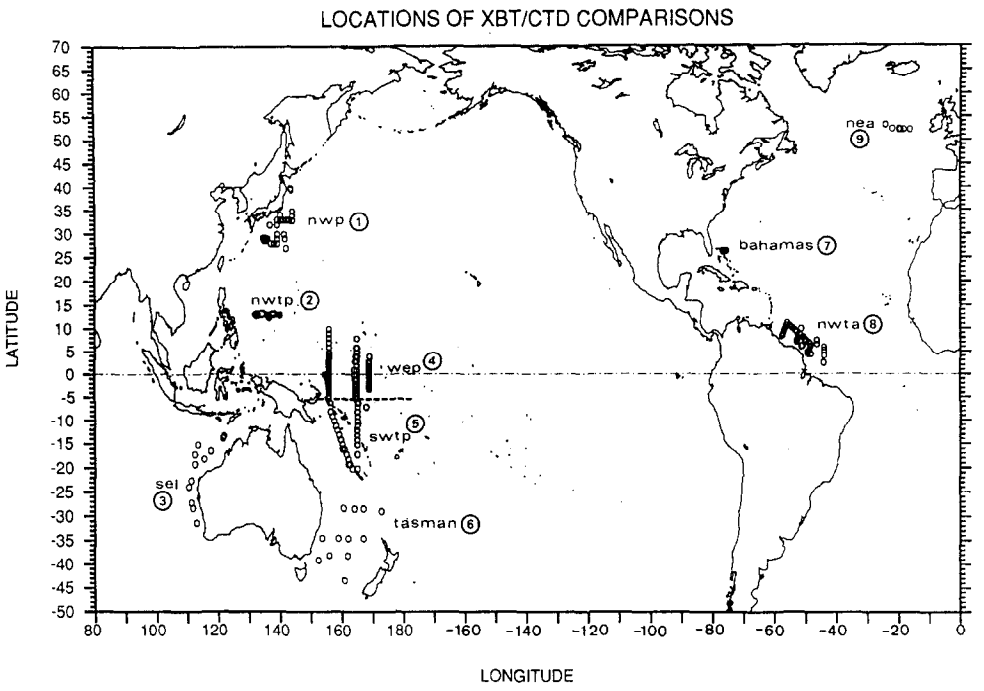

Fig. 1. Locations where the XBT/CTD comparison experiments were conducted (see also Table 1). The dashed line at 5°S in the western Pacific shows the limit between the wep and swtp data sets.

to temperature. In this study we will only examine the depth errors associated with inaccuracies in the fall rate equation.

For a given type of probe, the depth–time equation provided by the XBT manufacturers is of the form

$$z_m = a_m t - b_m t^2 \tag{1}$$

where z_m is the depth and t is the elapsed time in seconds starting when the probe hits the surface; a_m and b_m are positive constants. The linear coefficient is a function of the hydrodynamic characteristics of the probe in the water and the quadratic coefficient is a function of the change in mass of the probe (unreeling of the wire) and of the change with depth of the water characteristics (density and viscosity gradients; see Green, 1984).

The method

Hanawa and Yoritaka (1987) and Hanawa and Yoshikawa (1991) first developed a temperature-error-free method for determining errors in the depth–time equation. The essence of the method is that comparison to the field standard should be made not for the absolute temperature profiles but for the temperature gradient profiles. This is because temperature errors are directly related to depth errors, and bias-like temperature errors can be eliminated by using the temperature gradient information. The detection method

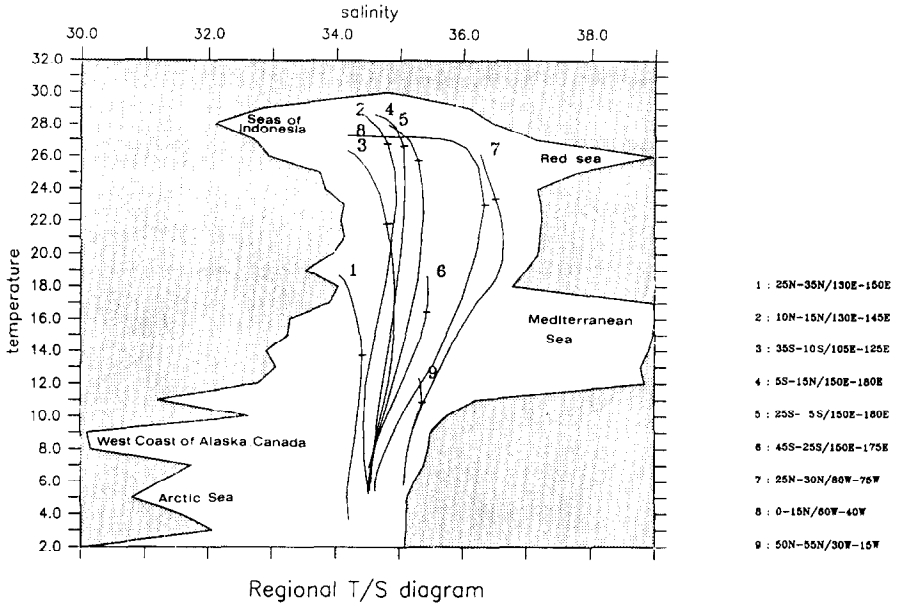

Fig. 2. Temperature–salinity (T–S) diagrams from the climatological data (Levitus, 1982). Curves 1–9 represent the field areas of the comparison experiment (see Fig. 1 and Table 1). A 100-m mark has been added to each curve. The shaded area limits the T–S field of the world's open oceans down to 800 m.

adopted for the depth error in the present analysis is an extension of this method. It was first independently developed by Hanawa and Yasuda (1992) and Rual (1991), and is further simplified and modified here for better accuracy. The detection procedures used in the present analysis for obtaining depth errors are as follows.

Step 1, *The* 1-m-*interval data*. The 1-m-interval data are calculated using a linear interpolation scheme for both raw CTD and XBT temperature data. Here, the CTD pressure is converted into depth by using the approximate equation (2) of Hanawa and Yoritaka (1987), calculated for a σ–t of 27.5:

$$z_{\mathrm{ctd}} = 0.993\, p_{\mathrm{ctd}} \tag{2}$$

where z_{ctd} is the CTD depth in metres and p_{ctd} is the CTD pressure in decibars. The XBT depths, z_{m}, are calculated from the depth–time equation (1) provided by the XBT manufacturer.

Step 2, *Filtering*. The raw XBT and CTD data inevitably contain vertically small-scale geophysical and instrumental noise (e.g. spikes). Therefore, before applying the actual detection procedures, two filters are applied to the raw data (Rual, 1989): (i) a non-linear Median filter known to eliminate completely the spikes in a signal, (ii) a low-pass linear cosine Hanning filter to smooth out the small-scale noise. In the present analysis, a seven-point Median filter without threshold logic is adopted. This filter can eliminate the spikes which consist of up to three data points (width of 2 m, see Sy, 1985, and Brock, 1986, for details). After application of the Median filter, a simple three-point Hanning filter, with weights of 1/4, 1/2, 1/4, is applied nine times (equivalent to a more sophisticated 11-point

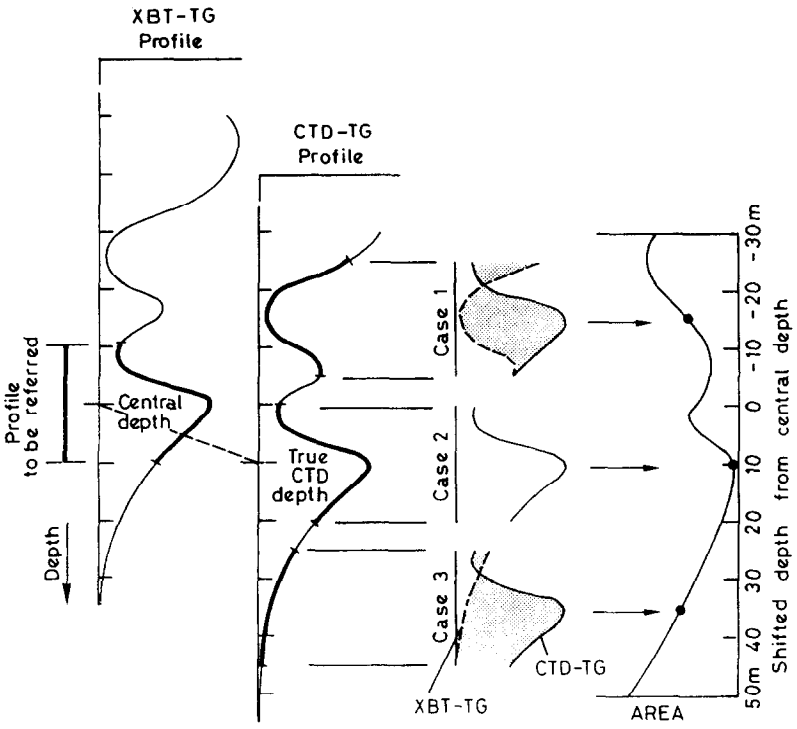

Fig. 3. Explanatory picture of the detection method adopted to determine the XBT depth error (adapted from Hanawa and Yasuda, 1992). See *Step* 4, in the text, for further details.

Hanning filter applied once). As a result, small-scale undulations with wavelengths less than about 5 m are also eliminated with a minimum of transfer to longer wavelengths (see Blackman and Tukey, 1958 for details).

Step 3, *Calculation of temperature gradient*. Temperature gradients (TG hereafter) are calculated every metre from both filtered CTD and XBT data.

Step 4, *Detection of actual depth*. Reference XBT depths are defined at fixed XBT-depth intervals (i.e. at fixed elapsed times from the surface). For each of these reference XBT depths a fixed length depth-window defines a segment on the XBT temperature gradient (XBT-TG) profile. A corresponding depth-window, initially centred on the same depth, is shifted up and down along the CTD-TG profile until the area between the CTD and XBT segments of the temperature gradient profiles is minimized (see Fig. 3). The central depth of the shifted CTD segment, which gives the minimum value of this area, can be regarded as the actual depth of the reference XBT central point. The depth-shift of the CTD segment is the corresponding depth-correction. Therefore the elapsed time of the reference XBT central point can then be paired with its actual CTD depth to provide the corrected XBT depth–time data necessary for the calculation of the fall rate equation in the next step. In the present analysis, the depth-window is 50 m wide, and its shifting range is from 30 m above the central depth to 50 m below it, by 1 m steps. The estimates of the XBT depth are made at 25 m intervals from 100 m to the maximum depth (z_M). At less than 100 m, the temperature gradient is often constant

or rapidly varying with internal waves leading to too many errors in the estimation. Thus n_M, the maximum possible number of depth–time pairs (or of depth differences) calculated for a given profile, is

$$n_M = 1 + (z_M - 100)/25 \tag{3}$$

This procedure can be automated, but a visual quality control of the depth-difference profiles is required in order to eliminate non-coherent depth-differences due to problems in the temperature profiles themselves.

Step 5, *Estimation of individual depth–time equations*. After the visual elimination of the non-coherent depth differences and of their corresponding depth–time pair, the individual a_i, b_i coefficients for each profile are then determined by the method of least squares from the remaining corrected depth–time pairs:

$$z_i = a_i t - b_i t^2 \tag{4}$$

In the present analysis, coefficients calculated for profiles with less than 2/3 of n_M (equation (3)) have been eliminated. This elimination of the a_i and b_i calculated from an inadequate number of depth–time pairs is necessary to ensure the accuracy of the individual coefficients by providing a sufficient depth range, especially important for the b coefficient which characterizes the curvature of the profile.

Step 6, *Estimation of the new depth–time equation*. Using the coefficients a_i and b_i from the profiles with a sufficient number of "good" depth–time pairs, the mean coefficients, A and B, are calculated:

$$Z = At - Bt^2 \qquad \text{where } A = \text{mean } (a_i) \text{ and } B = \text{mean } (b_i). \tag{5}$$

Remarks on the present method. In Hanawa and Yoritaka (1987) and Hanawa and Yoshikawa (1991), temperature gradient extreme have been chosen as markers to detect depth differences. In that case, it is relatively difficult to evenly distribute the data points from the surface to the bottom of the profile. This is because the existence of the extrema completely depends on the characteristic shapes of the temperature profiles. On the other hand, the present method can be applied to any temperature profile irrespective of the existence of extrema, and the data points are evenly distributed over the whole depth range. The only restriction is that the temperature gradient must not be constant but has to change, at least slightly, within the search range of *Step* 4, in order to allow determination of a depth-shift minimizing the area between the XBT and CTD temperature gradient profiles.

In Hanawa and Yasuda (1992), after the depth-error detection in *Step* 4, there was an additional step to recalculate the XBT time matching a given true XBT depth. In addition, three more steps and an iteration were necessary after the calculation of the *tentative* revised equation before the determination of the *final* equation. The main difference between their method and our method is that their revised equations were calculated by a least square fit to the whole set of depth–time pairs calculated from all the profiles. They did not take into account the fact that all the depth–time pairs of a given profile are related by a relationship expressed by a depth–time equation specific to the profile (or by the coefficients a_i and b_i).

Another advantage of the present method is the easy addition of new data sets to a previous estimate of the mean A and B coefficients. Since the coefficients of equation (5) are the mean of all the individual coefficients, to add a new data set is simply to calculate

the mean coefficients of the new data set (*Steps* 1 to 5) and to take the weighted mean of the two estimates. Thus this newly adopted method is simpler and more accurate than the previous method. It is more automatic, and demands only visual inspection of the depth-difference profiles to flag the depth–time pairs (*Step* 4). However, the new method does also occasionally fail to detect depth differences when the vertical temperature gradient is constant in a section of the profile larger than the search window, or when the XBT temperature profile has features not matched by the CTD profile.

Depth-error distribution on the plane of the a *and* b *coefficients*

The a–b *plane: maximum depth-error isolines.* As shown in Hanawa and Yasuda (1992), it is possible to determine for a given depth range (depending upon the probe type) the maximum absolute depth difference between a reference depth–time equation (coefficients A and B) and any other depth–time equation (coefficients a and b). As fully described in Appendix 1 of UNESCO (1994), this maximum absolute depth error is not always located at the same depth (Fig. 4a), and therefore a maximum relative depth error may be a better representation. However, this relative error may reach a maximum at the surface where the absolute depth error is zero. The best representation may therefore be the maximum absolute depth error expressed as a relative depth-error (i.e. divided by its depth).

Isolines for any of these depth errors can be calculated and plotted on the plane of all the a and b coefficients (called hereafter the a–b plane). The construction and calculation of such plots is given in UNESCO (1994). An example of a T-7 a–b plane, with a maximum depth of 800 m, is shown in Fig. 4b. Isolines are given as a percentage of the depth at which is located the maximum absolute error. In order to show the difference between the maximum absolute depth error and the same error relative to its depth, ±8 m isolines (1% at 800 m) are also given. The five depth error curves in Fig. 4a correspond to the *ab* points (Fig. 4b, 1 to 5) lying on the horizontal line passing through the Sippican *ab* point (5). As seen in Fig. 4a, depending upon the a–b coefficients, the maximum depth-error is positive or negative, and is located either at the maximum depth of the profile or at the depth where the vertical gradient of the error is zero. This leads to two types of "iso-error" curves (see Fig. 4b) and the loci of the transitions between these two types of errors are two straight lines: (i) the "transfer" line (T in Fig. 4b) where the vertical gradient of the error is null at the maximum depth (Fig. 4: curve 4 and *ab* point 4); (ii) the "discontinuity" line (D) where the error (2) at the maximum depth (800 m), expressed as a percentage, is equal, but of opposite sign, to the "zero-gradient" error (here at 277 m), also expressed as a percentage (2). These two lines divide the a–b plane into four sectors. In the upper-left and lower-right sectors the depth of the maximum error is the maximum depth of the profiles (1 and 5), whilst in the two other sectors this depth is variable within a certain depth range (2, 3 and 4, with depth respectively of 800/277 m, 400 m and 800 m). More remarkable in these last sectors is the consistency of the depth along any line issued from the reference AB point (dotted lines from 800 to 300 m every 100 m). The only zero-error point on the a–b plane is the reference AB point. Along the "discontinuity" line the variation of the depth error is at a minimum due to the depth-error curve (2) occurring more or less symmetrical about the zero-error axis. The isolines define a central area, elongated along the "discontinuity" line, where the maximum depth error is small even when the a and b coefficients are largely different from those of the reference equation. Therefore, if the coefficients of individual

profiles or individual data subsets are distributed within this depth-error region, the error may be within the instrumental noise and a unique depth–time equation can be computed.

Therefore, by using the *a–b* plane, one can (i) see at a glance whether or not an *ab* point is within the manufacturer's specification, (ii) determine its maximum depth error, (iii) depending upon the sector, determine the error type and the depth of the maximum error.

Statistics on the a–b *plane.* Generally, the individual *ab* points, calculated in *Step* 5, can be considered as samples of two correlated quasi-normal variables (see again Appendix 1 of UNESCO, 1994). Any treatise on bi-variate statistics shows that the confidence interval of such a bi-variate normal distribution is represented by an ellipse centred on the mean *AB* point, and its equation is a function of the correlation coefficient r between a and b and of the standard deviations of each variable. The probability for an individual *ab* point to be in the area enclosed by an ellipse of n standard deviations is less than for a single normal variable, and one must refer to tables of the cumulative bi-variate normal density function (such as Abramowitz and Stegun, 1972) to calculate it. However, if n and r are high enough ($n \geq 2$ and $r > 0.5$), the confidence levels are close to those of a single normal variable. Hereafter these ellipses will be called the "individual" statistical ellipses (see Figs 6 and 7).

The statistical distribution and the confidence interval of the mean *AB* point can moreover be represented by a "mean" statistical ellipse (using the standard error of the mean). It has the same confidence level as the original ellipse, and its axes have the same directions as the axes of the corresponding original ellipse, but they are divided by the square-root of the number of points used to calculate that mean. The "mean" ellipse is in fact the probable area where the actual mean lies, so it can be considered as the actual "size" of the calculated mean (Fig. 6).

QUALITY CONTROL OF THE DATA

Mechanical application of the detection procedures described in the previous subsection will be adequate only for ideal XBT/CTD comparison data. Actual XBT data sometimes include imperfections due to problems such as bowing and wire stretching (see Bailey *et al.*, 1989, 1994; Sy, 1991). In addition, temperature profiles themselves are sometimes inappropriate for comparison, for instance, regions where the temperature gradients are constant over a wide depth range. Therefore, an inspection of the comparison data for imperfections is required. In this subsection, examples will be shown to demonstrate the effect of such problems on the procedures.

Figure 5 shows three typical examples of XBT/CTD comparisons: O7A16, C7B08 and T7A03. Generally, the temperature gradient profiles of the CTD and XBT correspond well to each other, for example O7A16. On the other hand, C7B08 is an example obviously affected by a bias-like temperature error, but the temperature gradient profiles of the XBT and CTD nevertheless correspond well to each other. The XBT depth-error profile of O7A16 is seen to be monotonically increasing from −2 m at 100 m to −22 m at 750 m,

Fig. 4. Depth errors of *T*-7 depth–time equations compared to the new reference equation (7) for *T*-4, *T*-6 and *T*-7 XBTs; (a) different types of error curves; (b) *T*-7 (800 m) *a–b* plane with maximum absolute depth-error isolines expressed in metres (dash-dotted lines), or in percent of their depth (full lines). Transfer (T) and discontinuity (D) dashed lines and iso-depth lines (dotted) are indicated. The 1 to 5 *ab* points along the horizontal line correspond to the 1 to 5 curves of (a).

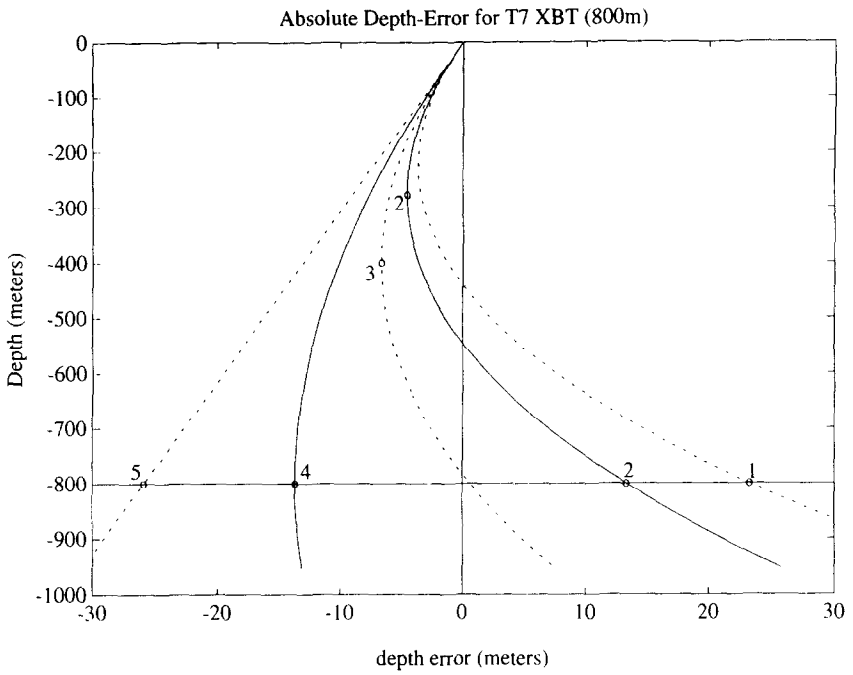
Absolute Depth-Error for T7 XBT (800m)
Depth (meters)
depth error (meters)
0
-100
-200
-300
-400
-500
-600
-700
-800
-900
-1000
-30
-20
-10
0
10
20
30
1
2
3
4
5

(a)

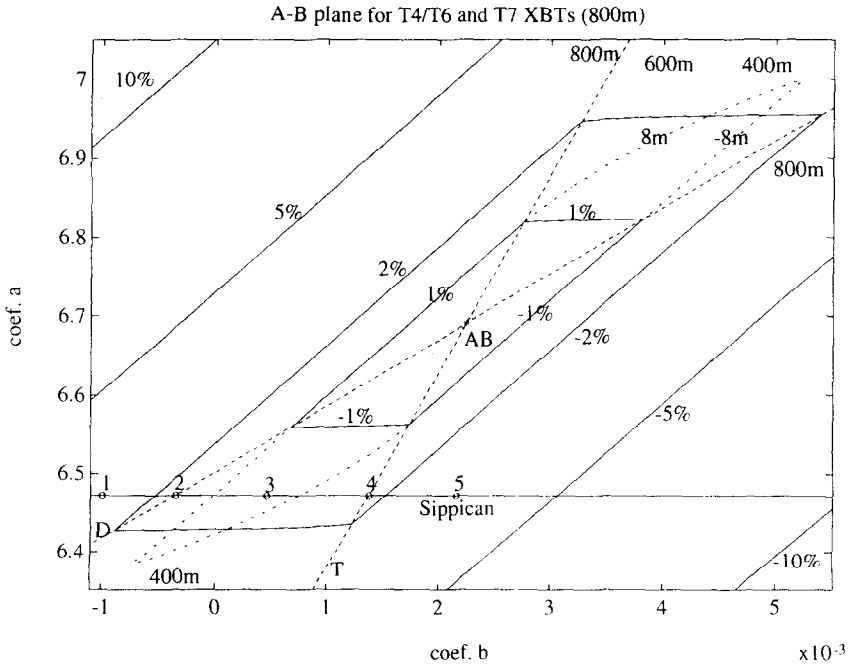
A-B plane for T4/T6 and T7 XBTs (800m)
coef. a
coef. b
x10-3
7
6.9
6.8
6.7
6.6
6.5
6.4
-1
0
1
2
3
4
5
10%
5%
2%
1%
-1%
-2%
-5%
-10%
800m
600m
400m
8m
-8m
AB
D
T
Sippican
1
2
3
4
5

(b)

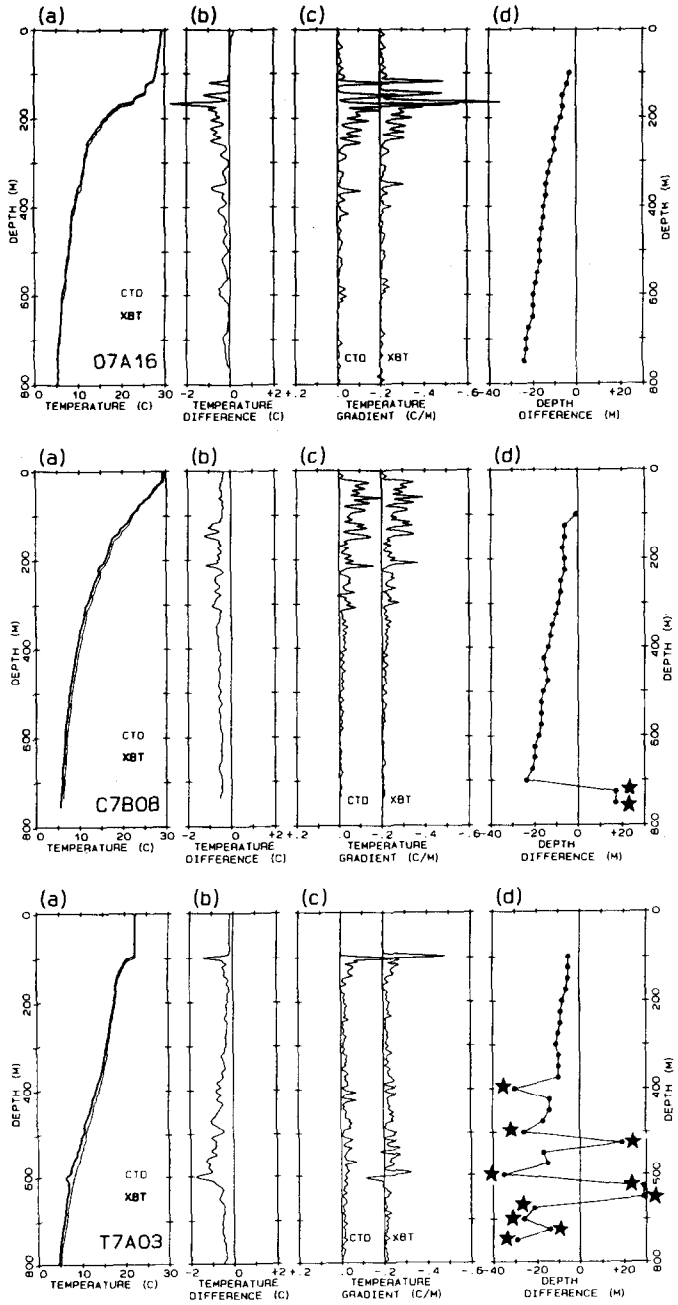

Fig. 5. Typical examples of comparison data: O7A16, C7B08 and T7A03. (a) CTD (thin line) and XBT (thick line) temperature profiles, (b) profile of the temperature difference (XBT minus CTD), (c) CTD and XBT temperature gradient profiles (XBTs are offset by −0.2°C/m), and (d) detected XBT depth errors. The depth errors marked by stars are considered non-coherent and consequently eliminated from the data set.

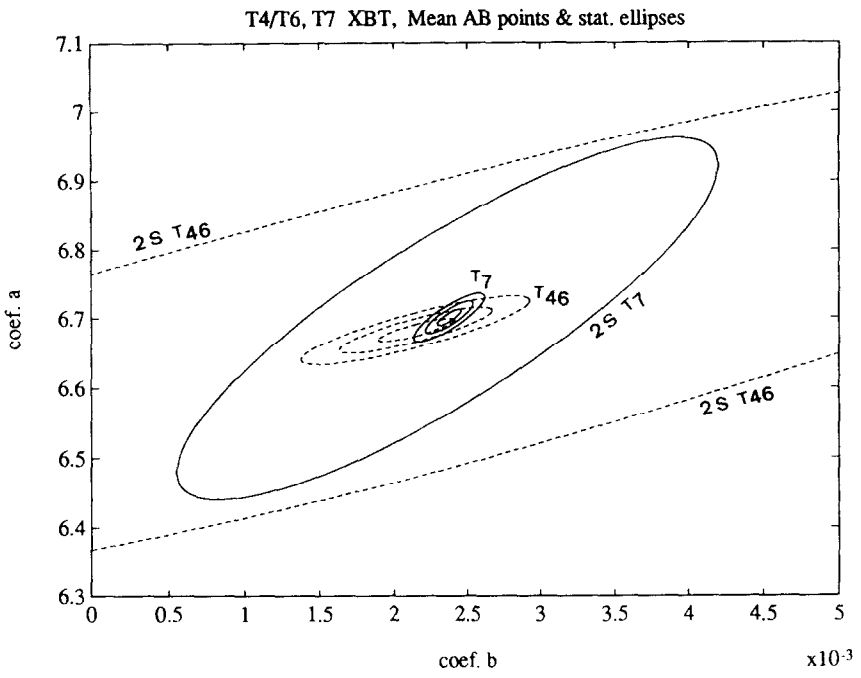

Fig. 6. Statistical ellipses on the a–b plane: individual two standard deviation ellipses (2S $T_{4/6}$ and 2S T_7), and one-, two- and three-standard-error-of-the-mean ellipses (T_{46} and T_7) for the global T-4/T-6 and for the global T-7 data sets (see Table 1).

whilst C7B08 is almost monotonically increasing from −1 m at 100 m to −22 m at 700 m. This example shows that, as already mentioned, this method can reasonably detect the depth difference even for XBT data having bias-like temperature errors. On the other hand, T7A03 not only includes a bias-like temperature error, but is probably also influenced by wire stretching and/or wire insulation penetration type defects, most obvious around 600 m. Therefore, the XBT temperature gradient profile does not correspond well to that of the CTD data, especially below 350 m, and it largely deviates and scatters in the depth-error profile from 400 m downward. In this case, such non-coherent deviations in the depth-difference data (marked by stars in the figures) are manually discarded at the end of *Step* 4 before the estimation of the individual equation in *Step* 5. In addition to the examples shown in Fig. 5, the detection of the depth error sometimes failed when the surface mixed layer was deeper than 100 m (constant temperature gradient). In such a case, the depth-difference data are also manually discarded after a visual inspection of the depth-difference profile. Due to the overall coherence of the depth-error profile, it is in general not difficult to determine which depth-difference data should be discarded from, or included in the analysis.

NEW REFERENCE DEPTH–TIME EQUATION FOR T-7, T-6 AND T-4 XBTS

The depth-difference data were estimated for 211 T-4/T-6 and for 161 T-7 XBT profiles. After examination of the depth-difference profiles, five of the T-7 XBTs were completely discarded from the analysis due to a general mismatch between the CTD and XBT profiles

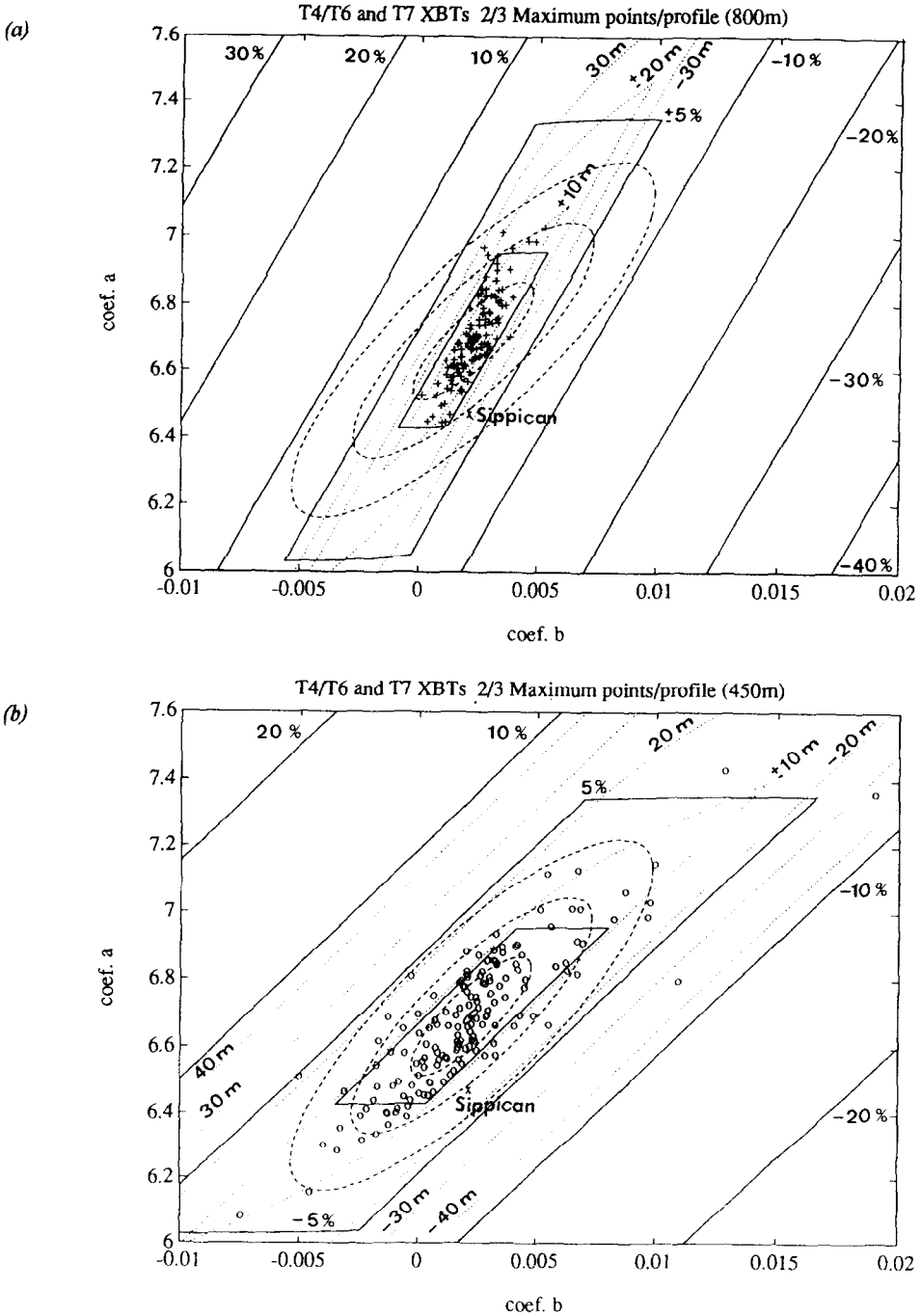

Fig. 7. (a) *T*-7 and (b) *T*-4/*T*-6 data sets presented on their respective *a*–*b* plane (800 m or 450 m maximum depth) of the new *T*-4/*T*-6/*T*-7 reference equation (7). The maximum absolute depth-error isolines are expressed in metres (dotted lines) or in percent of its depth (full lines), the central isoline is ±2%. The statistical ellipses are the individual one-, two and three-standard-deviation ellipses (dashed) and the small two standard-error-of-the-mean ellipse (full).

as a result of XBT malfunctions. Out of the remaining profiles, only 160 *T*-4/*T*-6 and 125 *T*-7 were considered as "good" profiles, following the "2/3 of n_M" criterion (see *Step* 4 and Table 1). Using the above "good" profiles, the individual a_i and b_i coefficients (*Step* 5) were first calculated. The new mean depth–time equations (*Step* 6) were then calculated independently for the *T*-4/*T*-6 and for the *T*-7 data sets (see Table 1 and UNESCO, 1994, for details), even though the manufacturers used the same original depth–time equation for *T*-4, *T*-6 and *T*-7 XBTs:

$$z_m = 6.472t - 0.00216t^2 \tag{6}$$

It is interesting to examine, on the same *a*–*b* plane, the two series of statistical ellipses for the *T*-4/*T*-6 and for the *T*-7 *ab* points respectively (Fig. 6). One can see that (i) the *T*-7 individual two-standard-deviation ellipse is completely embedded in the corresponding *T*-4/*T*-6 ellipse; (ii) the *T*-7 mean ellipses intersect with the corresponding *T*-4/*T*-6 ellipses. Thus the *T*-7 and *T*-4/*T*-6 populations and their means are not significantly different from a statistical point of view and we can safely determine a new reference equation for the combined data set:

$$Z_{467} = 6.691\ t - 0.00225\ t^2 \tag{7}$$

The confidence intervals for the individual a_i, b_i and for the mean A, B coefficients, at a confidence level of 95%, are

$$a_{467} = 6.691 \pm 0.354 \qquad b_{467} = 0.00225 \pm 0.00508$$
$$A_{467} = 6.691 \pm 0.021 \qquad B_{467} = 0.00225 \pm 0.00030$$

The normalized standard deviations of the mean, σ_A/A and σ_B/B are, respectively, equal to 0.16% and 6.7%. The quadratic term B is a corrective second order term and it is normal for it to be less accurately determined, especially when using shallow probes such as the *T*-4/*T*-6 probes.

Even though the manufacturers' rated depth is 760 m for the *T*-7 probe, the *T*-7 probe's actual maximum depth is very often over 800 m, whilst the *T*-4/*T*-6 XBTs actual maximum depth is very close to the manufacturers' rated depth of 460 m. Therefore 800 m and 450 m will be considered as the maximum depths of the *T*-7 and *T*-4/*T*-6 *a*–*b* planes. The 367 individual *ab* points are presented in Fig. 7 on these AB_{467} planes. The dashed ellipses are individual one-, two- and three-standard-deviation ellipses for the a_ib_i points which, with a correlation coefficient of 0.83, correspond to confidence levels of 57% (and not 68% as for a single variable), 95% and 99.7% respectively. In Fig. 7a, the maximum depth errors for the individual *T*-7 probes and the individual one standard deviation ellipse for the AB_{467} reference point are mostly within the ±2% and ±10 m isolines, although some are outside the +20 m isoline. On the *T*-4/*T*-6 *a*–*b* plane (Fig. 7b), the *T*-4/*T*-6 individual points are more scattered, although the maximum depth errors are still generally within the 2% and ±10 m isolines, with several points just within the ±5% and ±20 m isolines. The manufacturer's equation ab_m point is outside the main cloud of observed *ab* points in both Figs 7a and 7b, at over two individual standard deviations from the AB_{467} reference point, in a sector where the maximum depth error is −26 m and −3.24% at the depth of 800 m, or −15 m and −3.26% at 450 m. A small two-standard-error-of-the-mean ellipse has been included to show the "size" of the mean AB_{467} point.

The *T*-7 and *T*-4/*T*-6 mean *AB* points (not shown) are within one standard error of the

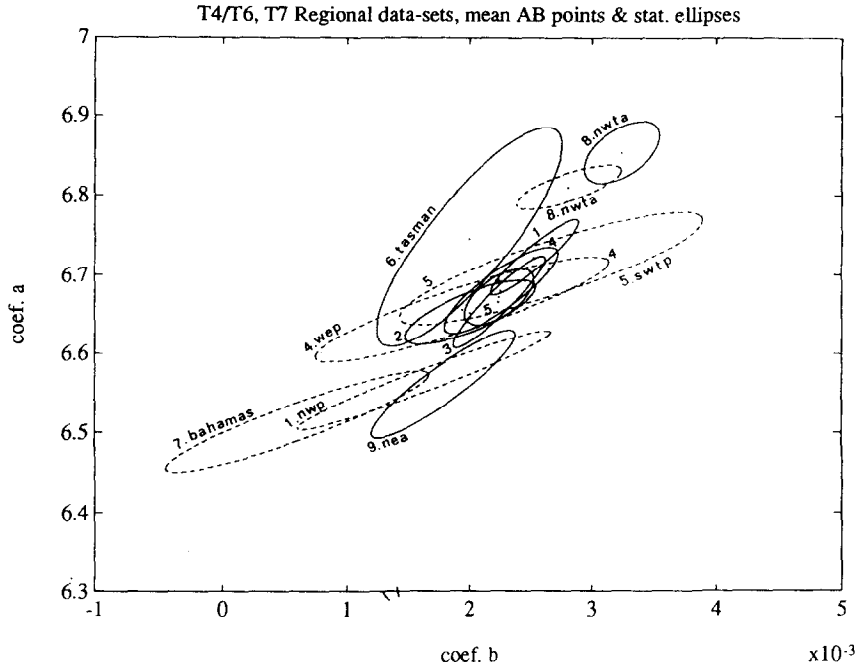

Fig. 8. Mean regional two-standard-error-of-the-mean ellipses on a zoomed *a–b* plane (see Fig. 1 and Table 1 for the location of the regions). The full and the dashed ellipses are, respectively, the *T*-7 and the *T*-4/*T*-6 mean regional ellipses. For clarity, in the medium group some ellipses are referred to by their region number only.

mean from the AB_{467} reference point (see Table 1). The maximum absolute depth error between the AB_{467} reference point and the *T*-7 *AB* point is −0.8 m or −0.1% at 800 m and for the *T*-4/*T*-6 *AB* point it is −0.2 m or −0.06% at 264 m. These results confirm that a single reference *T*-4/*T*-6/*T*-7 depth–time equation can replace, with very reasonable accuracy, the original manufacturers' equation.

INTER-COMPARISONS OF THE INDIVIDUAL DATA SETS

Regional comparisons

Figure 8 shows, on the *a–b* plane, the two-standard-error-of-the-mean ellipses (95%) of the mean *AB* points for each regional data set. These ellipses define three main significant groups whose domains do not intersect: (i) a slow fall rate group, which includes the *T*-7 north-eastern Atlantic (*nea*), the *T*-4 *Bahamas* and the *T*-6 north-western Pacific (*nwp*) data sets; (ii) a high fall rate group which includes the *T*-7 and the *T*-4/*T*-6 north-western tropical Atlantic data sets (*nwta*); (iii) a medium fall rate group which includes all the other regional groups, except the *T*-7 *Tasman* data set. The ellipse for this data set, which has only six probes, is too wide to belong to one group. It is mainly a high fall rate data set, but it also covers part of the medium group. The three groups appear to show no overall regional homogeneity. The slow fall rate group ranges from tropical latitudes to high latitudes in the northern hemisphere. The medium fall rate group is mainly a tropical and

subtropical group, but includes the *T*-7 north-western Pacific data set which is a mid-latitude data set. The Tasman data set, which is also a mid-latitude data set, ranges from medium to high fall rates. The *T*-6 and *T*-7 north-western Pacific data sets are found in different groups, i.e. the slow and medium fall rate groups respectively.

Although there were no opportunities to collect data in extreme oceanic conditions, the data presented in this study were collected in several different regions in order to examine the possible influence of different water masses on the fall rates of the probes. One of the parameters for understanding the dynamics of a moving body in water is viscosity (Seaver and Kuleshov, 1982). Viscosity is, to the first order, inversely proportional to the temperature; therefore the mean temperature over the water column may be used to represent the mean viscosity. Another parameter is the density, but in our case, the correlation is very high (−0.91) between the mean density and the mean temperature; therefore the results found for the mean viscosity are applicable to the mean density. Figure 9 presents the mean regional A and B coefficients as a function of this mean temperature calculated between the surface and the maximum depth reached by the probe type (800 m for *T*-7, 450 m for *T*-4/*T*-6). The expected influence, if any, should be a decrease in the speed of the probes (decrease of A mainly) with increasing viscosity. The only significantly different pairs of A coefficients are the north-western tropical Atlantic (*nwta*), a medium viscosity data set, and the north-eastern Atlantic (*nea*), a high viscosity data set, for the *T*-7; and the same *nwta* and the north-western Pacific (*nwp*) for the *T*-4/*T*-6 probes. For these two pairs of data sets the theoretical linear change in the fall rate is very close to the observed change of 0.3 m/s for the *T*-7 and 0.22 m/s for the *T*-4/*T*-6. But if other pairs of data sets are considered, an inverse relationship can be found (i.e. *nwp* and *nwtp* for the *T*-7, or *nwp* and *Bahamas* for the *T*-4/*T*-6). This may be due to the variability of the probe shape, or weight, generating different turbulent drags, completely obscuring the viscosity influence. In fact, considering all the regional data sets, it is very difficult to find a global relationship, and most of the regional A and B coefficients are not significantly different at a 95% confidence level.

Onboard equipment comparisons

The data sets in the medium fall rate group of Fig. 8 were collected by almost all of the different types of onboard XBT and CTD equipment used in the study (see Table 1). Therefore, no significant influence of the type of onboard system on the fall rate appears to exist. Moreover, in the north-western tropical Atlantic (*nwta*), in the north-western Pacific (*nwp*) and in the south-eastern Indian Ocean (*sei*), respectively, comparisons were made using, in the same area, the same type of XBT but different onboard systems (see UNESCO, 1994). No significant differences were observed in the fall rates for the *nwta* or for the *nwp* data sets, when the data were grouped by onboard equipment. The two-standard-error-of-the-mean ellipses are almost tangent for the *sei* case (not shown), but the two mean AB points are so close that the induced error is small (5 m at 800 m or 0.6%).

Probe manufacturer comparisons

Probes from two different manufacturers were used in this study. They should be identical as the TSK probes are made under licence from Sippican. The *T*-7 and the *T*-4/*T*-6 probes from each manufacturer are grouped together for comparison on the a–b plane in

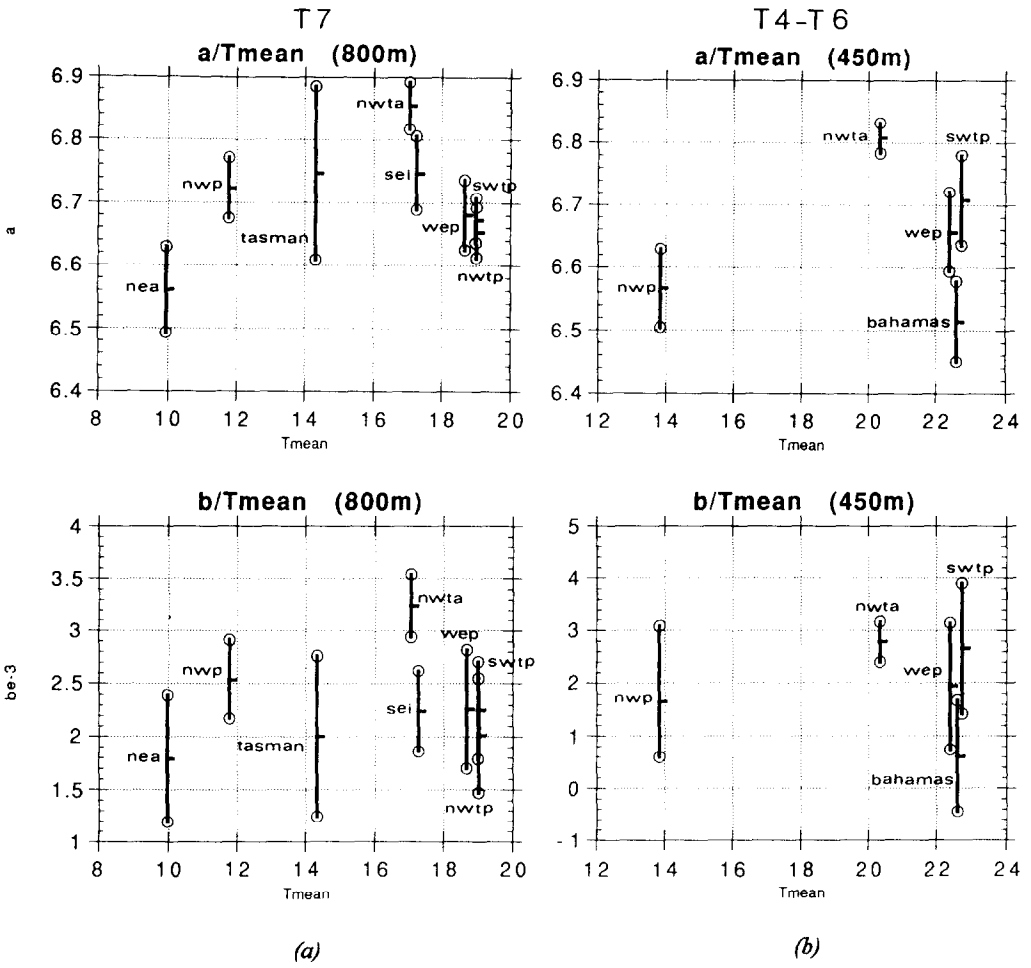

Fig. 9. The mean A, B coefficients and the two-standard-error-of-the-mean bars for the different regions of the XBT/CTD experiment are plotted against the mean temperature of the water between the surface and the maximum depth reached by the probe type (9a: 800 m for T-7, 9b: 450 m for T-4/T-6). See Fig. 1 for the location of the regions. The mean temperature has been computed from the Levitus (1982) T–S data of Fig. 2.

Fig. 10. The standard-error-of-the-mean ellipses (95%) show that the two T-7 data sets are quasi-identical. They have very close mean AB points, and their variability is comparable: there are 42 TSK T-7 *ab* points and 83 Sippican *ab* points, so the axes of the mean ellipses should have a theoretical ratio of 2/3, which is the case. The Sippican T-4/T-6 probes are not significantly different from the T-7 probes, but there seems to be a problem with the TSK T-6 probes (17 probes). This problem cannot be a batch problem as the probes were launched during two different cruises, 3 years apart. It cannot be a regional problem, as most of the TSK T-7 probes were launched in the same area and sometimes during the same cruise with the same onboard equipment. There seems to be a real but small difference between the TSK T-6 XBTs and the other probes: -6 m, or -1.3%, maximum depth error with the reference AB_{467} point.

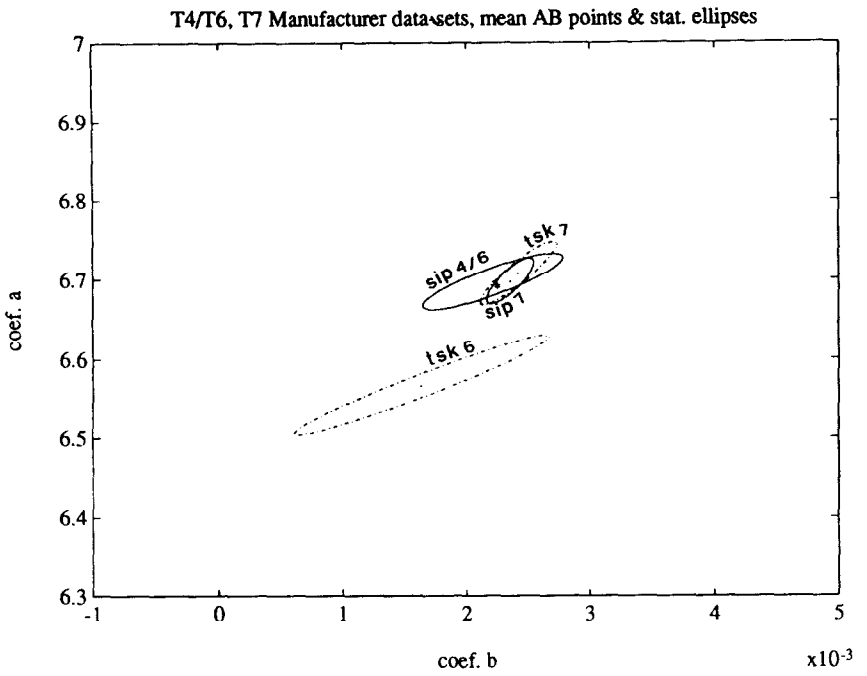

Fig. 10. Mean Sippican, and TSK, *T*-7 and *T*-4/*T*-6 *AB* points and their two-standard-error-of-the-mean ellipses on the *a*–*b* plane (same scales as Fig. 8, see Table 1 for detailed information).

Discussion on the inter-comparisons

Of the regional groups described above (Fig. 8), only the slow fall rate for TSK *T*-6 (*nwp*) may be explained by a statistically significant manufacturing difference. The location of the *Bahamas* data set in the slow fall rate group cannot be explained by density or viscosity effects, as one would expect these effects to result in it being in the medium fall rate group. As it is a single experiment using the same type of probes and onboard equipment used to collect some of the other data sets, the more plausible explanation is probe batch variation. Similarly, the north-eastern Atlantic data set (*nea*) is a single experiment, so its slow fall rate may be due to probe batch variations or, since it is the only experiment to use a Sippican Mk-12 onboard unit, it may be due to an onboard equipment influence. But since the high density and viscosity in the area favour a slow fall rate, this may be a regional influence. The high fall rate and the large mean ellipse of the Tasman Sea single experiment, on the other hand, may be a batch problem plus the fact that the area of the experiment actually spans over subtropical and mid-latitude frontal regions. The high fall rate of the two *T*-7 and *T*-4/*T*-6 north-western tropical Atlantic (*nwta*) data sets cannot be explained by any influence. It is a multi-cruise, multi-onboard equipment, multi-institution, multi-probe experiment, and the density and viscosity in the area favour a medium fall rate. So, if this high fall rate is real, it is due to an influence of unknown origin.

Therefore, only two differences between the data sets cannot be explained by batch variations: (i) the TSK *T*-6 probes' systematic slower fall rate; (ii) the north-western tropical Atlantic data set's high fall rate. However, these two differences have a very small influence on the overall combined data set, as the errors are symmetrical about the

reference AB_{467} point (about ±6 m or ±1.3% at 450 m) and the TSK *T*-6 data sets constitute a small number of the comparisons evaluated. In fact, if all the regional *AB* points are plotted on the global AB_{457} reference planes (Fig. 11 and Table 1), most of these points are inside or along the ±6 m maximum absolute depth-error isoline (or 1.3%), except the Tasman Sea (+10 m) and the north-eastern Atlantic (*nea*, −9 m). This is the maximum induced depth error if the regional depth time equations are replaced by the new reference depth time equation (7). It is well within the scatter of the individual probes (within the individual one-standard deviation ellipses of Fig. 7).

Moreover, if some differences were found in the means, all these differences are of practically no importance compared to the individual, or batch-to-batch, scatter of the probes (Fig. 12). All the individual regional two-standard-deviation ellipses intersect to the extent that the slow and fast fall rate groups are hardly discernible. So, if any other influences do exist, they are embedded in the individual or batch-to-batch fall rate variations of the XBT probes. Unless the manufacturers are able to reduce that variability, further regional experimentation will not be of interest, except perhaps in extreme oceanic conditions of density and viscosity.

OBSERVED VARIABILITY AND THE MANUFACTURERS' SPECIFICATIONS

In order to study the depth errors over the whole water column and not only the maximum depth error, one has to use the depth-error versus depth plane instead of the *a*–*b* plane. Figure 13a shows the distributions of the 5895 valid depth differences as a function of their CTD depth (as calculated in *Step* 4) for the combined *T*-4/*T*-6/*T*-7 data set. The elapsed times corresponding to the depth differences are identical for each profile, as the depth differences are determined every 25 "XBT metres" from the manufacturers' depth–time equation (6) in *Step* 1. Therefore all the depth differences at a given elapsed time can be grouped together to determine the depth-difference statistics for that given time (XBT depth). The corresponding CTD actual depths vary, as they are equal to the XBT depth plus the depth correction.

At each level the distribution of the depth differences are quasi-normal, and only a slight asymmetry in the scatter can be noted towards the high fall rate side of the distribution (high negative individual depth errors). The data are generally outside the manufacturers' specifications, except close to the surface where the mean depth error is within ±5 m down to a depth of 150 m. The mean depth errors range from −2.5 m at 100 m to −24.5 m at 775 m. Only the very slow fall rates, outside −1 standard deviation (about 15% of the data), are within the specifications almost down to the maximum depth. The observed scatter is much larger than expected from the manufacturers' specifications.

When the new *T*-4/*T*-6/*T*-7 equation (7) is used instead of the original manufacturers' equation (6) (Fig. 13b), the mean depth error is greatly reduced and is now within ±1 m of the CTD depth. However, 17.5% of the individual depth errors are still outside the manufacturers' specifications (1028 depth errors out of a total of 5895 depth errors). Only the one-standard-deviation confidence interval is entirely within those specifications, and one must reach the maximum depth for the two-standard-deviation curves to be close to the specifications. Between 100 m and 500 m, more than 10% of the depth errors are outside the specifications and up to 30% at 250 m (not shown). A linear approximation of the two and three-standard-deviation curves (dotted lines in Fig. 13b) gives

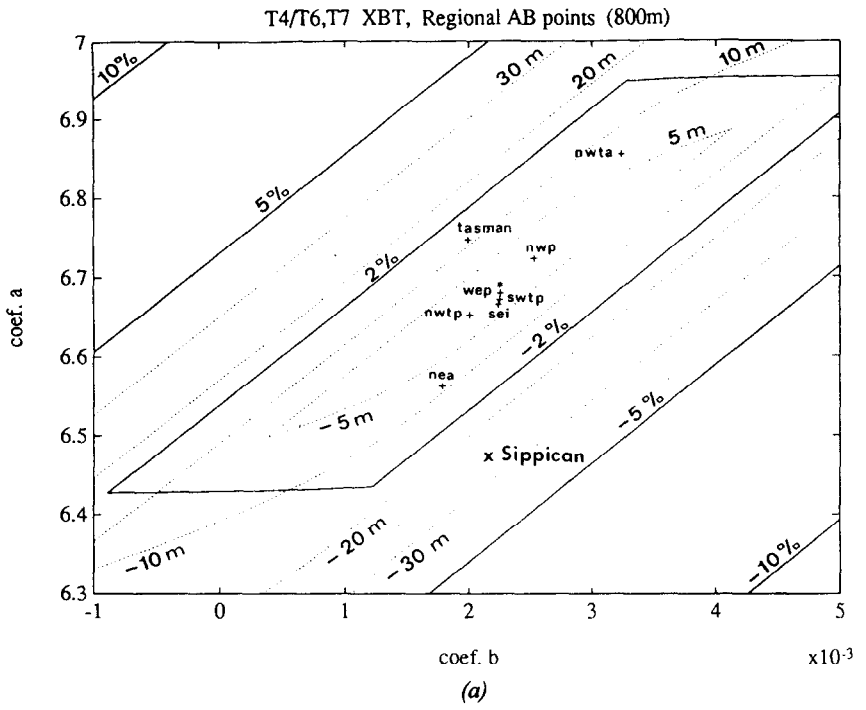

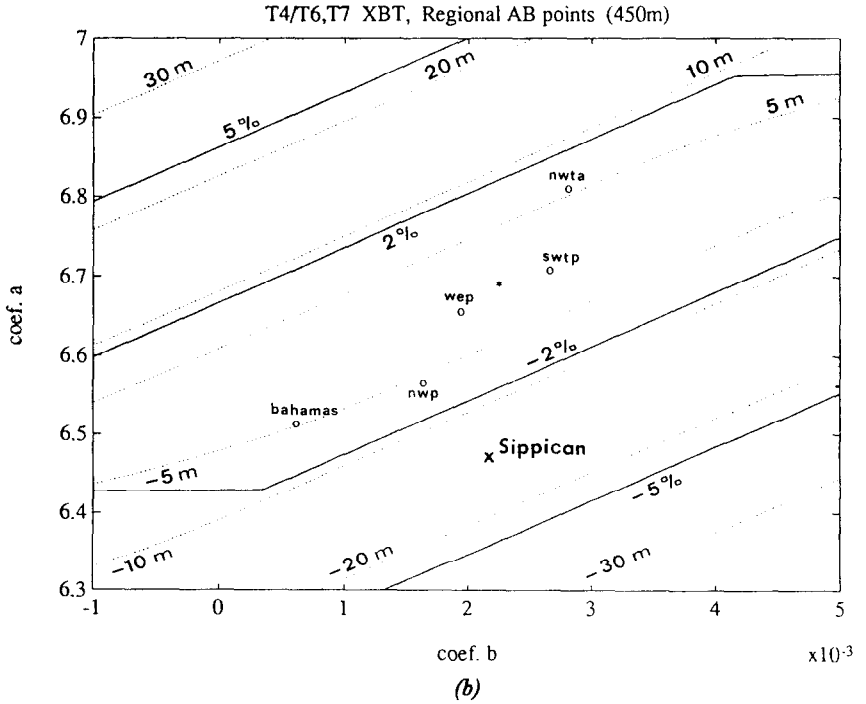

Fig. 11. Mean regional AB points on the new $AB_{4/6/7}$ reference planes of Fig. 7, but using the scales of Fig. 8. The reference AB point is marked by an *.

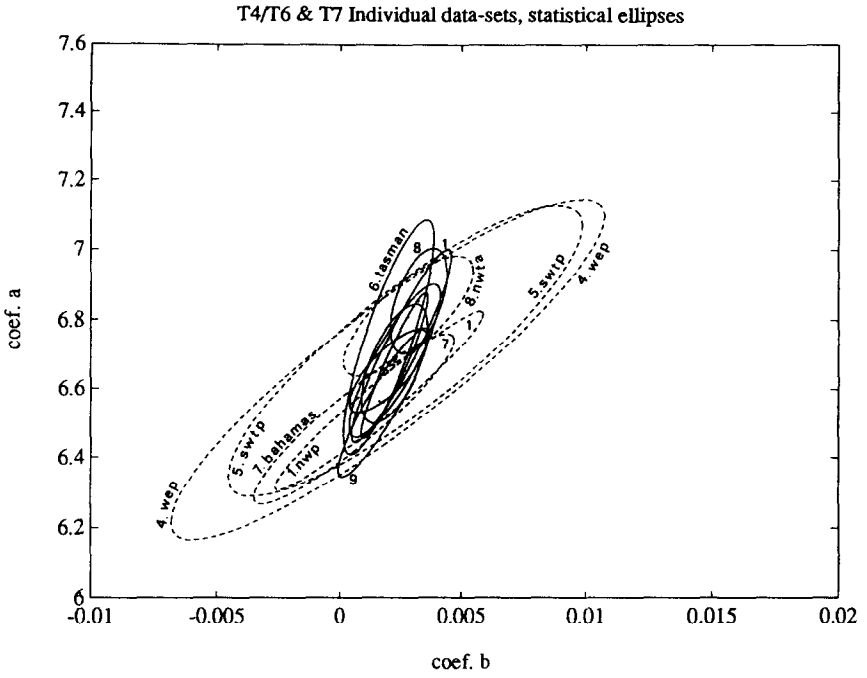

Fig. 12. Individual regional two-standard-deviation ellipses on the *a*–*b* plane (same scales as Fig. 7, see Fig. 1 and Table 1 for the location of the regions). The full and the dashed ellipses are, respectively, the *T*-7 and the *T*-4/*T*-6 individual regional ellipses. For clarity, in the central group some ellipses are referred to by their region number only.

$$\pm(6\text{ m} + 1.5\%\text{ of the depth}) \text{ for 2 std. dev. or } 95.5\% \text{ of the data} \quad (8)$$

$$\pm(9\text{ m} + 2.0\%\text{ of the depth}) \text{ for 3 std. dev. or } 99.7\% \text{ of the data} \quad (9)$$

If the meaning of a specification is that the depths of all the probes should be within them, then the specifications provided by the manufacturers should be at least close to the three-standard-deviation confidence interval. They should be of the order of equation (9). It must be noted that the new specifications are not $\pm n$ metres or $\pm p\%$, but $\pm(n$ metres plus $p\%)$. The shallow depth specifications therefore are much larger than they used to be: above ± 10 m at 100 m and around ± 15 m at 250 m instead of ± 5 m. Hallock and Teague (1992) found the same kind of probe-to-probe scatter after correction of the original data with their new equation: about ± 8 to 10 m in the depth range 10–100 m, and ± 15 to 20 m in the range 450–650 m.

The linearity of the standard deviation curves with depth is a good index of the reliability of the method used to calculate the depth errors. All over the depth range, the relative

Fig. 13. Combined *T*-4/*T*-6/*T*-7 data set: depth errors and their statistics as a function of depth. (a) Using the manufacturers' depth–time equation (6). Mean depth error (open circles) and the one-, two- and three-standard-deviation curves (respectively dotted, dash-dotted and full curves). The individual depth errors above two standard deviations are also added (dots). The manufacturers' specifications (± 5 m or $\pm 2\%$ of the depth, whichever is the greater) are indicated as dotted lines. (b) Same figure, but using the new *T*-4/*T*-6/*T*-7 reference equation (7). Linear approximations of the two- and three-standard-deviation curves are indicated as dotted lines.

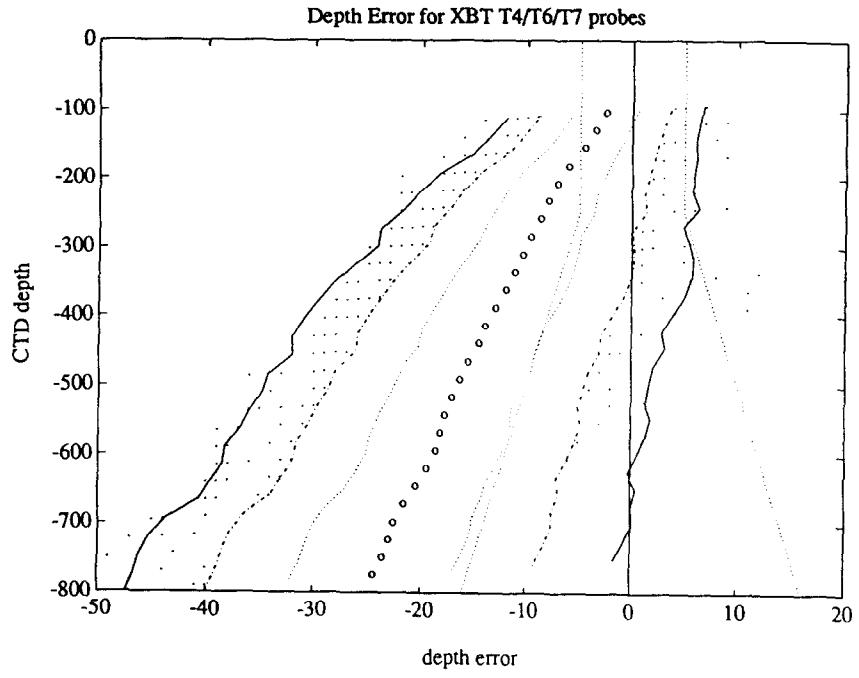
Depth Error for XBT T4/T6/T7 probes
CTD depth
depth error
0
-100
-200
-300
-400
-500
-600
-700
-800
-50
-40
-30
-20
-10
0
10
20

(a)

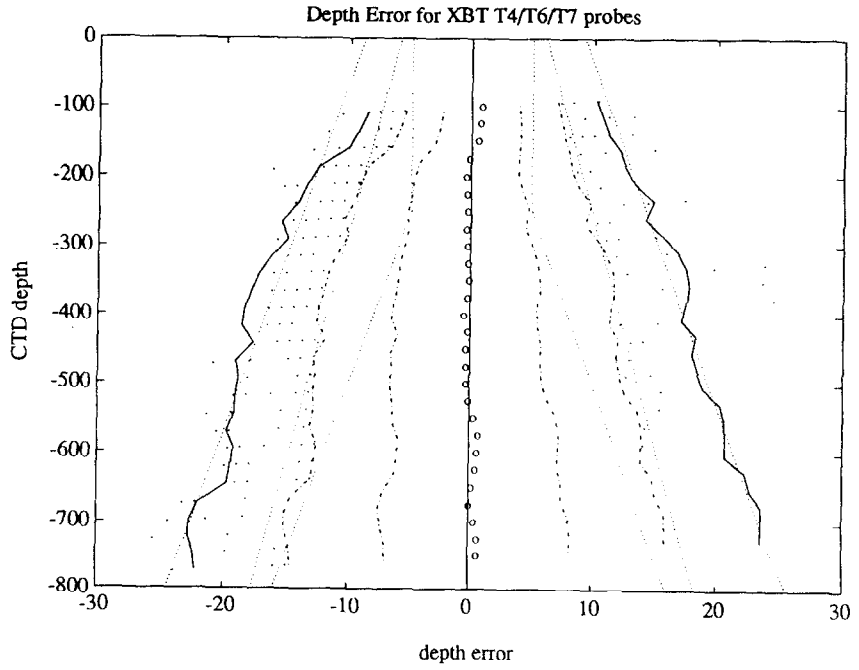
Depth Error for XBT T4/T6/T7 probes
CTD depth
depth error
0
-100
-200
-300
-400
-500
-600
-700
-800
-30
-20
-10
0
10
20
30

(b)

scatter of the probes remains constant, about 1.5% of the depth at a 95% confidence level. Therefore, if the general behaviour of the probes with depth remains similar from probe to probe, the reliability of the method remains constant whatever the depth, even when the vertical temperature gradients change only slightly.

If, instead of the total 5895 depth-difference data set, we consider only the 5340 depth differences used to determine the mean A_{467} and B_{467} coefficients of equation (7), the results are almost identical (not shown). Even the extreme data points (above three-standard deviations in Fig. 13) are not eliminated, as they are part of some of the "good" profiles. The mean depth error is still within ± 1 m, and the standard deviations are very slightly different, but the conclusions remain the same.

COMPARISON WITH OTHER AUTHORS' DEPTH–TIME EQUATIONS

Singer (1990) made a comprehensive review of the articles published prior to his own publication. Table 2 is a summary of the latest major experiments known to the present authors. All of the experiments were XBT/CTD comparison experiments, except Gould (1991), who compared the XBT depth when the probe hits the bottom to the depth of the bottom as measured by a precision echo-sounder. He also used Plessey *T*-7 probes which are not examined in our study, but which are supposed to behave the same way as the Sippican *T*-7 XBTs. The only other non-Sippican probe experiment was made by Yoshida *et al.* (1989) who used TSK *T*-7 probes. Most of the probes are *T*-7 XBTs, except Henin (1989) who used *T*-4 XBTs. Yoshida's Japan Sea experiment was made down to a maximum depth of only 300 m, so his TSK *T*-7 XBT results are more comparable to those for *T*-4 XBTs. The shallow (0–325 m) linear correction from Heinmiller *et al.* (1983) can also be placed into the same group. The majority of the experiments were made at relatively low latitudes, although Sy and Ulrich (1990), Gould (1991) and Yoshida *et al.* (1989) made their measurements at higher latitudes in colder waters. No studies have been made in Arctic or Antarctic waters. The 1976–1978 Sargasso Sea experiments (McDowell, 1977; Heinmiller *et al.*, 1983) were made with strip-chart recorders. Green (1984) used the same data as Heinmiller *et al.* (1983), but added a hydrodynamic model to define his two-coefficient depth–time equation. The latest publications, Yoshida *et al.* (1989), Sy and Ulrich (1990), Gould (1991), Hallock and Teague (1992), used temperature-error-free methods to calculate the depth errors. In the other publications, the authors tried to estimate the temperature error prior to the estimation of the depth error, and the result is accordingly less accurate. Another problem encountered in the earlier experiments is the non-exact simultaneity in time or space between the CTD and the XBT deployments, which allowed additional errors in the depth comparisons due to vertical displacement of features in the temperature field by internal waves and other high frequency space and time scale phenomena.

Table 2 also shows the maximum depth differences between the previous authors' equations and the new reference *T*-7/*T*-4/*T*-6 depth–time equation (7). The maximum depth differences for the *T*-7 experiments down to 800 m are from +13 m (1.6%) to −15 m (−1.9%). For the *T*-4s, or *T*-4-like *T*-7 experiments, the maximum depth differences down to 450 m are from +7 m (1.6%) to −6 m (−1.4%) and −18 m (−4%) for Heinmiller's 2s, the worst case, very close to the manufacturers' equation. In Fig. 14, the previous authors' results are presented on the *a*–*b* plane to show their relationship to one another and to the new AB_{467} reference point. Most of the earlier authors simply

Table 2. Summary of XBT depth comparison experiments made by previous authors

n°	Author	Date	No. of XBT	Probe type	Manu-facturer	Field experiment: Date	Field experiment: Area	XBT recorder	Depth reference	Linear correct.	A	B 10^{-5}	C metres	Maximum depth error: metres	Maximum depth error: %	A	B 10^{-5}
x	Sippican	1965		*T*-4	Sippican	?	?	?	?		6.472	216	—	−15	−3.26		
				T-6										−15	−3.26		
				T-7										−26	−3.24		
				DB										−26	−3.24		
1	McDowell	1977	47	*T*-7	Sippican	1976	Sargasso S.	Strip ch.	Plessey	1.020	6.601	220	—	−10.5	−1.3		
2s	Heinmiller	1983	139	*T*-7	Sippican	1976/78	Sargasso S.	Strip ch.	NB Is[a]	0.995	6.440	215	−1.1	−18.0	−4.0	6.367	108
2d	*et al.*								[b]	1.044	6.757	226	−17.1	−9.5	−1.1	6.330	−25
3	Singer	1990	14	*T*-7	Sippican	1985	G.Mexico	SA–810	NB III	1.0435	6.754	225	−4.3	3.6	0.5	6.617	131
			15	*T*-7	Sippican	1986	G. Mexico	Mk-9	"								
4	Henin	1989	35	*T*-4	Sippican	1987	W Trop. Pac.	Argos	SBE 9	1.050	6.796	227	—	7.1	1.6		
5	Sy & Ulrich	1990	11	*T*-7	Sippican	1989	Norw. Trench	SA–810	NB III	1.020	6.601	220	—	−10.5	−1.3		
				DB													
6	Gould[c]	1991	29	*T*-7	Plessey	1990	Iceland Faroes Ridge	SA–810	Echo-sounder	1.050	6.796	227	—	12.8	1.6		
7	Hallock & Teague	1992	118	*T*-7	Sippican	1990	Barbados	Mk–9	NB III	—	6.798	238	−4.0	7.3	0.9	6.669	149
8	Yoshida *et al.*[d]	1989	22	*T*-7	TSK	1988	Japan Sea	Z60II	NB IIIb	—	6.674	329	—	−6.1	−1.4		
9	Green[e]	1984	139	*T*-7	Sippican	1976/78	Sargasso S.	Strip ch.	NB Is	—	6.450	131	—	−15.4	−1.9		

Linear correction from 0 m to 325 m[a]
Linear correction from 326 m to 760 m[b]
True depth detected by a precision echo-sounder[c]
0–300 m XBT/CTD comparison (no temperature gradient below)[d]
Same data as Heinmiller & al, plus an hydrodynamic model[e]

The *ab* point numbers of Fig. 14 are given in column 1. The last eight columns are respectively (i) the linear-correction coefficients used by several authors to correct the manufacturer's equation (6), (ii) the *A* and *B* coefficients of the author's equation plus, when existing, a constant term *C* (offset at the surface), (iii) the maximum absolute depth error between the new reference equation (7) and the author's equation, (iv) the *A*, *B* coefficients of a two-coefficient equation (5), equivalent, by least square fit, to the author's three-coefficient equations.

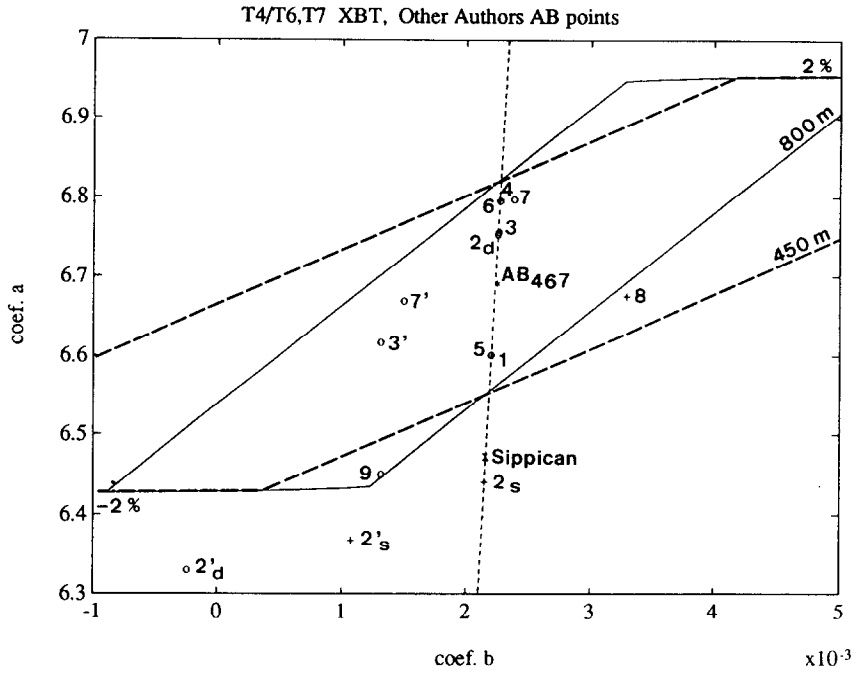

Fig. 14. Other authors' results (see Table 2 column 1 for the identification numbers) on the *a–b* plane of the new reference equation (7): (i) the circles are the *T*-7 *ab* points; the crosses mark the *T*-4, or *T*-4-like (2s and 8) *T*-7 *ab* points. The 2s', 2d', 3', and 7' *ab* points are from a re-calculation of the three-coefficient equations into two-coefficient equations. (ii) The long-dashed and the full line maximum absolute depth-error isolines are the ±2% isolines defined in Fig. 7, respectively, for the *T*-7 and *T*-4/*T*-6 *a–b* planes. The almost vertical short-dashed line is the [00, A_sB_s] line is the locus of any linear correction of the manufacturers' equation (6).

calculated a linear correction coefficient to correct the manufacturers' equation (6), so the representative *ab* point is on a linear curve [00, A_sB_s] linking the origin of the *a–b* plane to the manufacturers' *AB* point. The Hallock and Teague (case 7) *ab* point and our AB_{467} reference point, while differently determined, are nevertheless very close to the linear correction locus. The Yoshida (case 8) and Green (case 9) *ab* points have *b* coefficients far away from the linear correction curve. For the Yoshida case, this may be due to the special density structure of the Sea of Japan which has no temperature gradient below 300 m. The maximum depth for comparison in that study is therefore 300 m, and perhaps the quadratic coefficients can not be well defined due to the short depth range. For the Green case, which uses the same data as Heinmiller (2s and 2d), it could be caused by a problem in a parameter evaluation of his model.

Several authors who used the linear fit for their correction also found at the surface an extrapolated offset between −1 m and −17 m (see Table 2). In order to be able to compare their two results with the others on the *a–b* plane, we fitted a three-coefficient equation (5) by the method of least squares to their 3-coefficient equation ($z = at - bt^2 + c$), thus eliminating the constant term *c*. The additional error due to this approximation is small: between −1 m and +2.5 m in the depth range from 100 to 750 m. The corresponding revised coefficients are given in Table 2. The original coefficients without the constant

term are also presented in Fig. 14 for comparison. Apart from the deep linear fit of Heinmiller *et al.* (Table 2, case 2d, depth range: 326–750 m), which gives a constant term of −17 m extrapolated to the surface, all the other offsets at the surface are in the range −1 m to −4.5 m. Hallock and Teague (1992) and Singer (1990) discuss the issue of such offsets in more detail. Our results show no significant extrapolated offset near the surface (see Fig. 13b). If the probes do behave differently close to the surface, we are unable to address the problem with our experiments and procedures as we did not define depth-difference information in the first 100 m.

There seems to be no regional influence in the results from the previous authors. The identical 6 and 4 *ab* points are respectively in the cold North Atlantic and in the warm western tropical Pacific. The 1 and 5 *ab* points are also identical, but they are from the Sargasso Sea and from the Norwegian Trench respectively. Cases 3 and 7, which are very close, are from the western tropical Atlantic, but cases 1, 2s, 2d and 9 are also from the same area. There is perhaps a strip-chart recorder influence since all the corresponding *ab* points (1, 2s, 2d, 9) are in a slow rate group, but as they are also all from the Sargasso Sea this may be a regional effect. The other authors' results are generally about twice as far away from the AB_{467} reference point as our regional AB points (Fig. 11). This may be due to probe batch variability, to differences in the methods or in the equipment, to the non-simultaneity of the launches, or sometimes to a regional variation as may be the case for the Sea of Japan data from Yoshida *et al.* (1989).

In conclusion, most of the earlier authors' results fall within the ±2% depth-error isoline around our AB_{467} reference point. The exception is the Heinmiller *et al.* (1983) result, but their data when re-interpreted by Green (1984) fall within the same envelope. Therefore our results do not contradict most of the previous results, but improve their accuracy and extend their applicability to a greater part of the world's oceans.

DEPTH-CORRECTION FORMULA FOR ARCHIVED XBT DATA

In order to correct the depths of already archived XBT data, a correction formula, function only of the archived depth (z_m), has been presented in UNESCO (1994). The correction curve for the probes considered in this paper is almost linear, thus only a linear correction approximation will be presented here. As the linear coefficients are a function of the maximum depth of the probe and of the type of maximum depth error considered, there are two sets of linear coefficients: one set for the 800 m maximum depth probe type (*T*-7), the other for the 450 m maximum depth probe type (*T*-4/*T*-6). Each set is formed of three coefficients, one for each type of maximum depth error: absolute, relative and absolute expressed as a relative depth error.

For the global *T*-4/*T*-6/*T*-7 data set down to 800 m, the best linear coefficients (see UNESCO, 1994) are between 1.0336 to 1.0337 depending upon the depth error considered, and between 1.0337 and 1.0338 down to 450 m. As the probe type is currently not recorded with the archived data, it is advantageous to choose only one global linear coefficient for the *T*-4/*T*-6 and the *T*-7 probes. In order to minimize the absolute depth error while keeping the relative depth error within reasonable bounds in the first hundreds of metres, the best linear approximation (Z_1) adopted for correcting the depth is

$$Z_1 = 1.0336 z_m \tag{10}$$

The maximum errors induced by using this linear coefficient are less than −0.1 m at 800

m for the *T*-7 probes, and less than 0.05 m at 300 m for the *T*-4/*T*-6 probes. The relative depth error is less than ±0.03% for all depths. Thus the linear correction approximation is very accurate for these probes, but this may not be always true for other probe types and other manufacturers.

CONCLUSIONS AND RECOMMENDATIONS

Further evidence was found in this study that TSK and Sippican *T*-7, *T*-6 and *T*-4 XBT probes fall faster than the rate given by the manufacturers' depth–time equation, and that the resulting depth errors are outside the manufacturers' specifications. The *T*-4/*T*-6 and the *T*-7 data sets were found not to be statistically different at the 95% confidence level. Therefore a unique new reference *T*-4/*T*-6/*T*-7 fall rate equation was conclusively determined by a temperature-error-free method applied to a number of XBT/CTD comparison data sets which were collected in three oceans and under controlled conditions. Unfortunately, there were no opportunities to collect comparison data sets in polar regions or other extreme oceanic conditions. No significant regional, onboard equipment, or probe manufacturer influence on the fall rate was detected, except perhaps a regional influence in the north-eastern Atlantic, and a manufacturing difference in the TSK *T*-6 probes. Any influences, if they do exist, are masked by the individual variability of the probes, especially of the *T*-4/*T*-6 probes. This variability is well outside the manufacturers' specifications, even when the mean depth error is corrected to less than ±1 m by using the new *T*-4/*T*-6/*T*-7 reference depth–time equation. The main source of XBT depth variability seems to be the probe-to-probe or batch-to-batch variability of the probes' characteristics. The reason for this variability is undetermined. A review of the results published by previous investigators, which are generally from a single geographical area, leads to the same conclusions but with a larger variability.

It should be noted that the other types of Sippican–TSK probes, as well as probes produced by other manufacturers such as Sparton of Canada, will also need careful independent evaluation. It is important that each probe type (including different manufacturers) be evaluated to avoid inconsistencies occurring in the depth accuracies of XBT data stored in the national and international data centres. Indeed, until an international mechanism is established to implement general use of a new equation for the *T*-7, *T*-6 and *T*-4 XBTs, and until the equation used for depth determination, the probe type, and the probe manufacturer can be distinguished in the data archives, it is strongly advised that for the present time all XBT data sent to the national or international data centres include depths calculated from the original manufacturer's equation only. The existence of mixed data in the databases must be absolutely avoided.

Acknowledgements—The support of the International Oceanographic Commission and of the World Meteorological Organisation is acknowledged, as well as the input of John Withrow and the help of Melanie Jenard. Sippican Inc. provided technical and background information. We are also indebted to all those involved in the field acquisition and in the processing of the data.

REFERENCES

Abramowitz M. and A. Stegun, editors (1972) *Handbook of mathematical functions, with formulas, graphs, and mathematical tables*. Dover Publications, New York, 9th edition.

Bailey R. J., H. E. Phillips and G. Meyers (1989) Relevance to TOGA of systematic XBT errors. In *Proceedings*

of the Western Pacific International Meeting and Workshop on TOGA COARE, Noumea, 1989. J. Picaut, R. Lukas, and T. Delcroix, editors, Centre ORSTOM de Noumea, New Caledonia, pp. 775–784.

Bailey R. J., A. Gronell, H. Phillips, E. Tanner and G. Meyers (1994) Quality control cookbook for XBT data. *CSIRO Marine Laboratories Report*, **221**, 81 pp.

Blackman R. B. and J. Tukey (1958) *The measurements of power spectra*. Dover Publications, New York.

Brock F. V. (1986) A non-linear filter to remove impulse noise from meteorological data. *Journal of Atmospheric and Oceanic Technology*, **3**, 51–58.

Flierl, G. and A. R. Robinson (1977) XBT measurements of the thermal gradient in the MODE eddy. *Journal of Physical Oceanography*, **7**, 300–302.

Gould W. J. (1990) Depth error in *T*-7s. *WOCE Newsletter*, **10**, 10–11.

Gould W. J. (1991) RRS *Charles Darwin* Cruise 50, *IOMSDL Cruise Report*, **221**, 41 pp.

Green A. W. (1984) Bulk dynamics of the expendable bathythermograph (XBT). *Deep-Sea Research*, **31**, 415–426.

Hallock Z. R. and W. J. Teague (1992) The fall rate of the *T*-7 XBT. *Journal of Atmospheric and Oceanic Technology*, **9**, 470–483.

Hanawa K. and H. Yoritaka (1987) Detection of systematic errors in XBT data and their correction. *Journal of the Oceanographic Society of Japan*, **32**, 68–76.

Hanawa K. and Y. Yoshikawa (1991) Re-examination of depth error in XBT data. *Journal of Atmospheric and Oceanic Technology*, **8**, 422–429.

Hanawa K. and T. Yasuda (1992) New detection method for XBT depth error and relationship between the depth error and coefficients in the depth–time equation. *Journal of Oceanography*, **48**, 221–230.

Heinmiller R. H., C. C. Ebbesmeyer, B. A. Taft, D. B. Olson and O. P. Nikitin (1983) Systematic errors in expendable bathythermograph (XBT) profiles. *Deep-Sea Research*, **30**, 1185–1196.

Henin C. (1989) Experimental error of the expendable bathythermograph in the western tropical Pacific. Paper presented at the first session of the TOGA XBT ad hoc Panel of Experts, Noumea, New Caledonia, June 1989, pp. 9 (unpublished manuscript).

Intergovernmental Oceanographic Commission (1992) *Summary report on the Ad Hoc Meeting of the IGOSS Task Team on Quality Control for Automated Systems, Marion, Massachusetts, U.S.A., 3–6 June* 1991. IOC/INF-888, pp. 144.

Levitus S. (1982) Climatological atlas of the world ocean. *NOAA Professional Paper*, **13**, 173 pp.

McDowell S. (1977) A note on XBT accuracy. *Polymode News*, **29**.

Rual P. (1989) For a better XBT bathymessage, onboard quality control, plus a new data reduction method. In *Proceedings of the Western Pacific International Meeting and Workshop on TOGA COARE, Noumea*, 1989. J. Picaut, R. Lukas, and T. Delcroix, editors, Centre ORSTOM de Noumea, New Caledonia, pp. 823–833.

Rual P. (1991) XBT depth correction. *Addendum to the Summary Report of the Ad Hoc Meeting of the IGOSS Task Team on Quality Control for Automated Systems, Marion, Massachusetts, U.S.A., June* 1991, IOC/INF-888 Add, pp. 131–144.

Seaver G. A. and A. Kuleshov (1982) Experimental and analytical error of the expendable bathythermograph. *Journal of Physical Oceanography*, **12**, 592–600.

Singer J. J. (1990) On the error observed in electronically digitized *T*-7 XBT data. *Journal of Atmospheric and Oceanic Technology*, **7**, 603–611.

Sy A. (1985) An alternative editing technique for oceanographic data. *Deep-Sea Research*, **32**, 1591–1599.

Sy A. and J. Ulrich (1990) North Atlantic ship-of-opportunity XBT programme, 1989 data report. *Wissenschaftlich-Technische Berichte aus dem Deutschen Hydrographischen Institut*, **1990–2**, p. 89.

Sy A. (1991) XBT measurements, *WOCE Operations Manual, Part* 3.1.3 *WHP Operations and Methods, WOCE Report*, **67/91**, 19 pp.

UNESCO (1994) Calculation of the depth equation of expendable bathythermographs by a new temperature-error-free method (Application to Sippican/TSK *T*-7, *T*-6 and *T*-4 XBTs). *UNESCO Technical Papers in Marine Science*, No. 67.